Dyes and Pigments 113 (2015) 702–708

Contents lists available at ScienceDirect

Dyes and Pigments

journal homepage: www.elsevier.com/locate/dyepig

Photophysical properties and photochemistry of a sulfanyl porphyrazine bearing isophthaloxybutyl substituents

Sebastian Lijewski [a], Mateusz Gierszewski [a, b], Lukasz Sobotta [c], Jaroslaw Piskorz [c], Paulina Kordas [a], Malgorzata Kucinska [d], Daniel Baranowski [e], Zofia Gdaniec [e], Marek Murias [d], Jerzy Karolczak [f, g], Marek Sikorski [b], Jadwiga Mielcarek [c, *], Tomasz Goslinski [a, *]

[a] Department of Chemical Technology of Drugs, Poznan University of Medical Sciences, Grunwaldzka 6, Poznan, Poland
[b] Applied Photochemistry Lab, Adam Mickiewicz University in Poznan, Umultowska 89b, Poznan, Poland
[c] Department of Inorganic and Analytical Chemistry, Poznan University of Medical Sciences, Grunwaldzka 6, Poznan, Poland
[d] Department of Toxicology, Poznan University of Medical Sciences, Dojazd 30, Poznan, Poland
[e] Institute of Bioorganic Chemistry, Polish Academy of Sciences, Z. Noskowskiego 12/14, Poznan, Poland
[f] Faculty of Physics, Adam Mickiewicz University in Poznan, Umultowska 85, Poznan, Poland
[g] Centre of Ultrafast Laser Spectroscopy, Adam Mickiewicz University in Poznan, Umultowska 85, Poznan, Poland

ARTICLE INFO

Article history:
Received 1 August 2014
Received in revised form
3 October 2014
Accepted 6 October 2014
Available online 14 October 2014

Keywords:
Macrocyclization
Porphyrazine
Spectroscopy
Fluorescence
Absorption
Singlet oxygen

ABSTRACT

A magnesium porphyrazine possessing isophthaloxybutylsulfanyl substituents in the periphery was synthesized and subjected to various photophysical studies, including optical absorption and emission measurements. Moreover, synchronous fluorescence spectra were recorded and a contour three-dimensional map of the excitation-emission of the studied porphyrazine was obtained. The porphyrazine macrocycle exhibited interesting solvatochromic effects in many different solvents. Upon excitation with visible light, it generated singlet oxygen with a low quantum yield, therefore when it was encapsulated in liposomes it exhibited no photocytotoxicity in the *in vitro* study on human carcinoma LNCaP cell line.

1. Introduction

Porphyrazines (Pzs) are synthetic analogues of naturally occurring porphyrins. The Pz macrocycle consists of four pyrrole rings linked together with azamethine groups [1]. Pzs show unique spectrochemical properties and potential applications in technology and medicine, especially as photosensitizers in photodynamic therapy (PDT) [2–5]. Pzs with peripheral sulfanyl substituents revealed enhanced solubilities and higher singlet oxygen generation yields [6–9]. The main limiting factors for Pzs application in PDT are their poor solubility in water, tendency to form aggregates and photochemical instability. These drawbacks may be overcome by modifying Pzs periphery [1,10] or by their encapsulation in various drug delivery systems, of which liposomal formulations and dendrimeric architectures have shown potential for other azaporphyrins [11,12].

In this study we report the synthesis and photochemical characterization of a novel sulfanyl magnesium(II) porphyrazine with isophthaloxybutyl substituents.

2. Experimental section

2.1. Materials

2.1.1. 2,3-Bis[4-(3,5-dimethoxycarbonylphenoxy)butylsulfanyl] maleonitrile (*3*)

Dimercaptomaleonitrile disodium salt (465 mg, 2.50 mmol) and dimethyl 5-(4-bromobutoxy)isophthalate **2** (2.15 g, 6.25 mmol) were dissolved in anhydrous methanol (50 mL). The reaction mixture was stirred under reflux for 6 h. The solvent was evaporated and the residual brown oil was chromatographed (dichloromethane: methanol, 50:1, v/v) to give **3** as yellow-brown oil (0.91 g;

* Corresponding authors. Tel.: +48 61 854 66 31.
E-mail addresses: jmielcar@ump.edu.pl (J. Mielcarek), tomasz.goslinski@ump.edu.pl (T. Goslinski).

http://dx.doi.org/10.1016/j.dyepig.2014.10.004
0143-7208/

54% yield), which when refrigerated tends to solidify to yellow amorphous solid. M.p. = 75–81 °C; R_f (dichloromethane: methanol, 50: 1, v/v) 0.56; UV–Vis (dichloromethane) λ_{max} nm (log ε) 318 (4.13), 343 (4.23); ^{1}H NMR (500 MHz, pyridine-d_5) δ 8.52 (s, 2H, C4′, ArH), 7.91 (s, 4H, C2′, C6′, ArH), 3.97 (t, ^3J = 6.0 Hz, 2H, $SCH_2CH_2CH_2\underline{CH_2}$), 3.87 (s, 12H, $COOCH_3$), 3.31 (t, ^3J = 6.5 Hz, 4H, SCH_2), 1.92 (m, 4H, $SCH_2CH_2\underline{CH_2}$), 1.91 (m, 4H, $SCH_2\underline{CH_2}CH_2$); ^{13}C NMR (125 MHz, pyridine-d_5) δ 166.5 (C = 0), 159.9 (CH_2–O–C, ArC), 132.8 (C–CO, ArC), 123.5, (ArC), 122.3 (CN), 120.5 (ArC), 113.5 (NC–C–S), 68.3 (O–CH_2, Bu), 52.8 ($COO\underline{CH_3}$), 35.4 (S–CH_2, Bu), 28.5 ($SCH_2\underline{CH_2}$, Bu), 27.4 ($SCH_2CH_2\underline{CH_2}$, Bu); MS (ES pos) *m/z* 693 $[M+Na]^+$, 709 $[M+K]^+$. MS (ES neg) *m/z* 705 $[M+Cl]^-$. Anal. Calc. for $C_{32}H_{34}N_2O_{10}S_2$: C, 57.30; H, 5.11; N, 4.18; S, 9.56. Found: C, 57.46; H, 5.62; N, 4.20, S, 9.54.

2.1.2. 2,3,7,8,12,13,17,18–Octakis[4-(3,5-dibutoxycarbonylphenoxy) butylthio]porphyrazinato magnesium(II) (**4**)

Magnesium turnings (11 mg, 0.45 mmol) and a small crystal of iodine were refluxed in *n*-butanol (10 mL) for 4 h. After cooling to room temperature, the reaction mixture was transferred using a syringe to a flask containing maleonitrile **3** (233 mg, 0.34 mmol), and was heated under reflux for 22 h. Next, the reaction mixture was cooled to room temperature, filtered through Celite, which was then washed with toluene. Solvents were evaporated in a rotary evaporator, which resulted in a dark blue residue, and was chromatographed using silica gel (dichloromethane: methanol, 50: 1, v/v) and reverse phase column chromatography (methanol, than dichloromethane) to give **4** as dark blue film (111 mg; 37% yield). R_f (*n*-hexane: ethyl acetate, 7: 3, v/v) 0.44; UV–Vis (dichloromethane) λ_{max} nm (log ε) 317 (4.77), 378 (4.89), 501 (4.17), 611 (4.45), 672 (4.94); ^{1}H NMR (500 MHz, pyridine-d_5) δ 8.50 (s, 8H, C4′, ArH), 7.87 (s, 16H, C2′, ArH), 4.59 (s, 16H, SCH_2), 4.34 (t, ^3J = 6.5 Hz, 32H, $COOCH_2$), 4.15 (s, 16H, $SCH_2CH_2CH_2\underline{CH_2}$), 2.35 (bs, 32H, $SCH_2\underline{CH_2}\underline{CH_2}$), 1.64 (m, 32H, $COOCH_2\underline{CH_2}$), 1.35 (m, 32H, $COOCH_2CH_2\underline{CH_2}$), 0.87 (t, ^3J = 7.5 Hz, 48H, $COOCH_2CH_2CH_2\underline{CH_3}$); ^{13}C NMR (125 MHz, pyridine-d_5) δ 166.0 (C = 0), 160.0 (CH_2–O–C, ArC), 158.3 (N=C Ar), 141.6 (C–S, Ar), 133.0 (C–CO, ArC), 123.2 (ArC), 120.2 (ArC), 68.8 (ArO-$\underline{CH_2}$), 65.8 ($COO\underline{CH_2}$), 35.7 (S–CH_2), 31.4, 29.3, 28.0, 19.9, 14.3 (CH_3); MS (MALDI) *m/z* 3378 $[M+H]^+$. HRMS (ESI) Calc. for $C_{176}H_{233}MgN_8O_{40}S_8$: 3378.4060, Found: $[M+H]^+$ 3378.4009. HPLC purity 96.22–100.00% (Supplementary Content).

2.2. UV/Vis measurements

All solutions containing **4** were prepared prior to their absorbance, steady-state fluorescence, and fluorescence excitation measurements. UV–Vis absorption spectra were recorded on a JASCO V-650 spectrophotometer in the spectral range from 300 nm to 800 nm, whereas the emission spectra (steady-state fluorescence excitation and emission spectra, synchronous fluorescence spectra and 3D fluorescence spectra) were recorded on a Jobin Yvon-Spex Fluorolog 3-22 spectrofluorometer. Fluorescence quantum yields were calculated using quinine sulphate in 0.05 M H_2SO_4 as a reference for $S_2 \rightarrow S_0$ emission (Φ_F^{st} = 0.546) [13] and using zinc phthalocyanine (ZnPc) in DMF (Φ_F^{st} = 0.17) [14] for $S_1 \rightarrow S_0$ emission. Fluorescence quantum yields were calculated according to the equation below:

$$\Phi_F = \Phi_F^{st} \frac{\int F_X\left(1-10^{-A_{st}}\right)}{\int F_{st}\left(1-10^{-A_X}\right)} \frac{(n_X)^2}{(n_{st})^2} F_k \qquad (1)$$

here, $\int F_x$ is the area under the emission curve of the sample, $\int F_{st}$ is the area under the emission curve of the standard, and A_x and A_{st} are the absorbance of the sample and standard at an excitation wavelength, respectively, n_x – the solvent refractive index for the sample, n_{st} – the solvent refractive index for the standard, F_k – the constant describing the instrumental factors, including geometry and other parameters, Φ_F^{st} is the value of fluorescence quantum yield of the standard.

Synchronous fluorescence spectra (SFS) were collected by simultaneous scanning using the excitation and emission monochromators, in the range from 290 nm to 750 nm at $\Delta\lambda$ = 10, 20, 30, 40, 60, 80, 100, and 120 nm. However, after the preliminary selection only the data collected for $\Delta\lambda$ = 20 nm were discussed below. A contour map of the emission-excitation of **4** was obtained in acetonitrile by recording the emission spectra in the range from 350 nm to 750 nm using the excitation wavelengths from 300 nm to 400 nm, spaced by 5 nm intervals in the excitation domain.

Fluorescence lifetime measurements were made at the Centre for Ultrafast Laser Spectroscopy in Poznan, with the respective fluorescence lifetime spectrophotometer setup. Time-Correlated Single Photon Counting (TCSPC) technique, previously described in detail elsewhere [15], was applied. Spectra-Physics pico/femtosecond laser system was used as the source of exciting pulses. This included a Tsunami Ti: sapphire laser, pumped with a BeamLok 2060 argon ion laser, which generated 1–2 ps pulses at a repetition rate of about 82 MHz and average power of over 1 W, tunable in the 720–1000 nm range. The repetition rate of the excitation pulses varied from 4 MHz to a single-shot by using a model 3980-2S pulse selector. Second and third harmonics of the picosecond pulse obtained on a GWU-23PS harmonic generator could be used for excitation, giving greater flexibility in the choice of the excitation wavelength. Elements of an Edinburgh Instruments FL900 system were used in the optical and control components of the system. The pulse timing and data processing systems employed a biased TAC model TC 864 (Tenelec) and a R3809U-05 MCP-PMT emission detector with thermoelectric cooling and appropriate preamplifiers (Hamamatsu).

2.3. Singlet oxygen generation study

A singlet oxygen generation assay was performed according to the procedure described in detail by Sobotta et al. [16]. Irradiation was performed at 671 nm according to the Q-band maximum wavelength of **4** in DMF.

Further we used a Jobin Yvon-Spex Fluorolog 3-22 spectrofluorometer with H10,330B-75 NIR-PMT module to determine the values of quantum yield of singlet oxygen generation of **4**. Macrocycle was excited at 380 nm in acetonitrile in order to record luminescence of singlet oxygen at 1270 nm.

2.4. Liposome preparation

1-Palmitoyl-2-oleoyl-sn-glycero-3-phosphocholine (POPC) and L-α-phosphatidyl-DL glycerol (chicken egg, PG) were purchased from Avanti Polar Lipids– INstruchemie (Delfizijl, Netherlands). Liposomes with **4** were prepared by a thin-film hydration method [17,18]. Appropriate amounts of the lipid solutions in chloroform (25 mg/mL) and **4** (0.8 mg/mL) were placed in glass test tubes, mixed and evaporated to dryness using a rotary evaporator. Films formed on the bottom of the glass test tubes were dried overnight in a vacuum at room temperature to evaporate any remaining chloroform. Subsequently, the dried films were hydrated with HEPES buffered saline solution (10 mM HEPES, *N*-(2-hydroxyethyl) piperazine-*N*′-(2-ethanesulfonic acid), 140 mM NaCl, pH = 7.4) and dispersed by vortexing for 10 min using a Vortex Genie 2 digital. Resulting liposome suspensions were passed 21 times through polycarbonate membranes with a pore diameter of 100 nm, using a

syringe extruder (Avanti Polar Lipids) to obtain unilamellar liposomes with a uniform size distribution. The molar ratio of the final liposome formulation was **4** (0.1): PG (2): POPC (8).

2.5. Biological studies

The biological activity of **4** was determined using the LNCaP human cancer cell line (prostate carcinoma). The cell line was obtained from the European Collection of Cells Cultures (ECACC, Salisbury, UK). Cells were cultured in DMEM medium without phenol red, supplemented with 10% FBS, 1% penicillin/streptomycin and 1% L-glutamine at 37 °C, in a humidified atmosphere containing 5% CO_2.

The light source used for illumination was a high power LED MultiChip Emitter (60 high efficiency AlGaAs diode chips, Roithner LaserTechnik GmbH, Vienna, Austria) with a light intensity of 2.2 ± 0.5 mW/cm^2 at 690 nm (irradiation dose after 20 min was 2.64 J/cm^2). The plates were exposed to light at a distance of 8 cm. The total spectral irradiance at the level of the cells was measured using an RD 0.2/2 radiometer with a TD probe (Optel).

The cytotoxic effect of the tested compound was determined in dark and light conditions. Cells were seeded in 96-well plates at the density 2 × 10^4 cells per well and incubated overnight under cell culture conditions. Then, the cells were washed twice with Phosphate Buffered Saline (PBS, Sigma Aldrich, St. Louis, MI, USA) and the tested compound at concentrations of 0.08; 0.16; 0.34; 0.68; 1.35; 2.70; 5.40 μM for **4** in a medium containing 2.5% Fetal Bovine Serum (FBS, Sigma Aldrich, St. Louis, MI, USA) was added to each of the wells. Free liposomes (PG(2): POPC(8)) were prepared as controls. Cells were incubated for 24 h and were washed twice with PBS, and fresh medium was added to each well. The plates were irradiated for 20 min and the cell viability was determined after 24 h.

The cell viability after the PDT treatment was evaluated by the MTT assay [19]. Namely, 170 μL of the reaction solution containing methylthiazolydiphenyl-tetrazolium bromide (Sigma Aldrich, St. Louis, MI, USA) solution (20 μL; 5 mg/mL PBS) in culture medium was added to each well. Then, the cells were incubated 2 h under cell culture conditions and the plates were centrifuged at 190 × g for 3 min. Formazan crystals were dissolved by adding 200 μL DMSO (POCh, Gliwice, Poland). The absorbance was measured at 570 nm with a plate reader (Biotek Instruments, Elx-800). Cell viability was calculated as a percentage of the control. The results are presented as the mean ± SD from two independent experiments.

3. Results and discussion

The first synthetic step was the alkylation reaction of 3-hydroxyisophthalic acid dimethyl ester **1** with 1,4-dibromobutane following an earlier reported procedure [20] (Fig. 1). Compound **2** was used in the subsequent reaction with dimercaptomaleonitrile disodium salt, giving a novel maleonitrile derivative **3**. Macrocyclization reaction using compound **3** led to the symmetrical magnesium porphyrazine **4**.

Novel compounds were characterized by UV–Vis, MS and various NMR techniques (^{1}H-^{1}H COSY, ^{1}H-^{13}C HSQC, ^{1}H-^{13}C HMBC) (see Supplementary Content). Pz **4** was carefully purified by column chromatography and further analyzed by HPLC. The detailed analysis of ^{1}H-^{1}H COSY spectra and ^{1}H-^{13}C HMBC long–range correlations are presented in the Supplementary Content.

3.1. Spectroscopic studies

The absorption spectra of **4** in selected organic solvents were shown in Fig. 2. Table 1 presents spectroscopic and photophysical

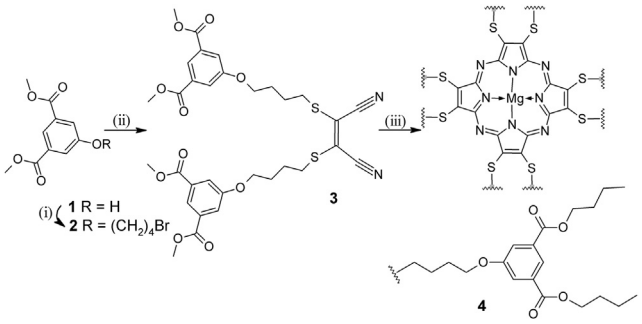

Fig. 1. Synthesis of compounds **2**–**4**. Reagents and conditions: (i) Br(CH$_2$)$_4$Br, K$_2$CO$_3$, DMF, 50 °C, 20 h [20]; (ii) (NC) (NaS)C=C(SNa) (CN), MeOH, reflux, 6 h; (iii) Mg(OC$_4$H$_9$)$_2$, *n*-BuOH, reflux, 22 h.

data for the singlet states of **4**, including absorption maxima for both the Soret and Q-bands (λ_1 and λ_2), emission maxima – noted for $S_2 \rightarrow S_0$ (λ_{F2}) and $S_1 \rightarrow S_0$ (λ_{F1}), and the fluorescence quantum yields (Φ_F). Two characteristic bands in the absorption spectra from 300 nm to 800 nm – the Soret band, located between 376 and 383 nm and the Q-band located between 664 nm and 681 nm were observed, and their exact positions were found to be dependent on the solvent used (see Table 1 for details). When analyzing the position of the Soret band in different solvents, it was concluded that the solvent polarity affects this band only weakly, whereas the changes noted in the Q-band were found to be more complex. In protic solvents (alcohols), its maximum was located at 670–674 nm, while in aprotic solvents at 664–681 nm. It is noteworthy, that the Q-band was found to be more intense than the Soret band, as it has been previously observed for other porphyrazine and phthalocyanine derivatives [21–23]. Both absorption bands correspond to π,π* electronic transitions. Table 1 presents the energy gap between the first and the second exited states. The largest energy gap was obtained in 1,4-dioxane and the smallest in dimethylformamide.

Fig. 3 presents the emission spectra recorded at different excitation wavelengths (λ_{exc} = 380 nm and 620 nm) and a synchronous fluorescence spectrum ($\Delta\lambda$ = 20 nm) of **4** in acetonitrile. Typically, the porphyrazine was excited with two excitation wavelengths (380 and 620 nm) in all solvents, upon which it emitted fluorescence. It was found that when the Pz **4** solution was excited at 380 nm, two fluorescence bands were observed, λ_{F2} peaking between 417 and 489 nm, and λ_{F1} peaking between 686 and 712 nm. The exact positions of these bands depended on the solvent (see

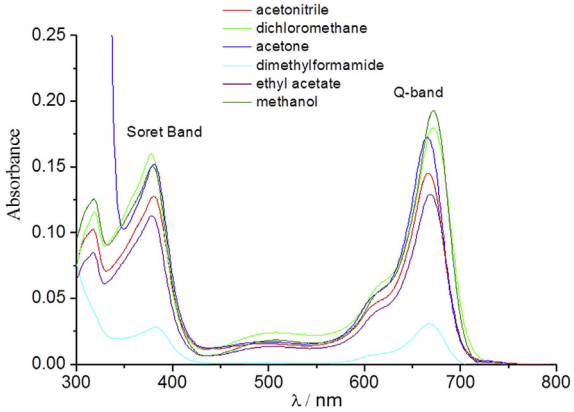

Fig. 2. Absorption spectra of **4** in different organic solvents (acetonitrile, dichloromethane, acetone dimethylformamide, ethyl acetate, methanol).

Table 1
Spectroscopic and photophysical data for the singlet states of **4**.

Solvent	λ_1/nm (Soret-band)	λ_2/nm (Q-band)	λ_{F2}/nm ($S_2 \rightarrow S_0$)	$\Phi_F \times 10^4$ ($S_2 \rightarrow S_0$)	λ_{F1}/nm ($S_1 \rightarrow S_0$)	$\Phi_F \times 10^3$ ($S_1 \rightarrow S_0$)	ΔE ($S_2 - S_1$)/cm^{-1}
cyclohexane	381	672	462	5.4	689	5.4	11,370
1,4-dioxane	376	681	489	4.8	712	3.2	11,910
ethyl acetate	378	666	422	4.2	689	9.7	11,440
dichloroethane	378	656	461	1.2	691	2.1	11,210
dichloromethane	378	674	458	1.1	697	2.4	11,620
dimethyl sulfoxide	380	672	436	3.1	691	4.5	11,430
dimethylformamide	383	667	421	3.6	686	5.4	11,120
acetone	380	664	453	6.2	686	1.2	11,260
acetonitrile	380	666	417	52.1	687	9.8	11,300
1-hexanol	379	674	423	9.2	690	6.2	11,550
1-pentanol	380	672	424	7.6	691	7.9	11,430
2-butanol	380	672	422	8.1	690	7.4	11,430
1-butanol	379	673	421	7.5	690	8.5	11,530
2-propanol	379	674	426	7.0	691	8.2	11,550
1-propanol	379	673	441	7.3	690	7.9	11,530
ethanol	379	671	426	6.9	690	7.4	11,480
methanol	379	670	427	5.6	692	6.7	11,460

Table 1). This short-wavelength emission band seems to correspond to the $S_2 \rightarrow S_0$ radiative transition, while the long-wavelength band to the $S_1 \rightarrow S_0$ radiative transition. Similarly, in the synchronous fluorescence and 3D fluorescence spectra, two emissions were observed. Notably, the long-wavelength emission maximum had the same location in the spectra excited by both 380 nm and 620 nm radiations.

In conventional luminescence spectroscopy, the emission spectrum is obtained by scanning the emission monochromator over various emission wavelengths, λ_{em}, at a particular constant excitation wavelength, λ_{exc}. The excitation spectrum is obtained by scanning the excitation over various wavelengths, and keeping the particular emission wavelength constant. Synchronous fluorescence spectrum (SFS) is obtained by simultaneously scanning both the excitation and emission wavelengths, keeping a constant difference between them. The synchronous fluorescence intensity (I_s) depends on various factors, including the concentration of the analyte in the sample (c), and may be expressed by the following equation:

$$I_s = KcbEx(\lambda_{exc})Em(\lambda_{exc} + \Delta\lambda) \quad (2)$$

Here, c – is the concentration of the analyte; Ex – intensity of the excitation spectrum at λ_{exc}; Em – intensity of the emission spectrum at $\lambda_{exc} + \Delta\lambda$; b – the thickness of the sample; K – is the constant describing the instrumental factors, including geometry and other parameters [24,25].

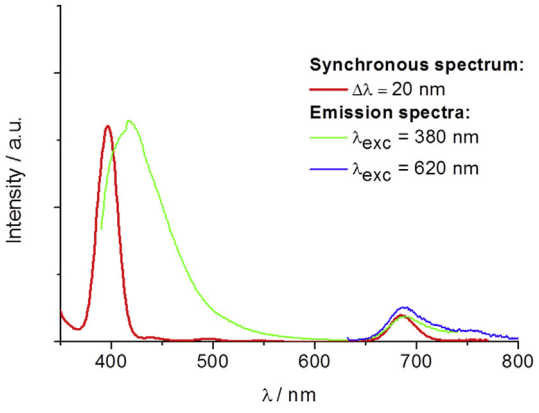

Fig. 3. Comparison between the synchronous fluorescence spectrum ($\Delta\lambda$ = 20 nm) and the emission spectra (λ_{exc} = 380 and 620 nm) in acetonitrile for **4**.

The SFS study was found to be particularly useful for acid-base equilibria in the ground and excited singlet states of various organic molecules, including lumichrome and quaternary stilbazolium salts [26,27]. Fig. 3 shows the two different bands in the SFS of **4** in acetonitrile. Noteworthy, SFS spectral bands are narrower than those in a conventional emission spectrum, with the two bands being clearly separated. The band with the maximum at about 397 nm seems to correspond to the $S_2 \rightarrow S_0$ transition, while the other at about 685 nm to the $S_1 \rightarrow S_0$ transition in all of the solvents used.

Similar results were obtained by Gan et al. [28] for a series of octaphenyl-porphyrazine-magnesium salts, with the emission from the S_1 state in THF observed at about 650 nm with the lifetimes of 1–3 ns, whereas the band emitting between 400 and 550 nm has been identified as the $S_2 \rightarrow S_0$ emission. The Φ_F of the S_2 emission was below 10^{-4}, while its lifetimes were too short for the nanosecond-resolution equipment. Interestingly, for a series of demetalated sulfur porphyrazines with polyetherol groups Ehrlich et al. [29] have reported dual fluorescence. Depending on the excitation wavelength, they observed the presence of short-wavelength emission coming from the S_2 state and at the same time the long-wavelength emission from S_1. Moreover, the intensity of $S_1 \rightarrow S_0$ emission significantly decreased with an increase of the number of sulfurpolyetherol groups. For porphyrazines with eight sulfurpolyetherol groups upon excitation at 350 nm short-wavelength emission was dominant and present at λ_{max} = 409 nm, and accompanied by very weak long-wavelength emission at λ_{max} = 745 nm. Porphyrazine with four sulfurpolyetherol groups excited at about 340 nm revealed two emission bands with maxima at about 424 nm and 823 nm. This observation was explained by a decrease of the S_1 emission accompanied by an increase of the number of sulfur atoms, because the radiationless conversion to the sulfur (n,π^*) state was present [29].

The excitation-emission map of **4** in acetonitrile exhibits a relatively intense broad band when the sample is excited between 300 and 325 nm and the emission monitored between 400 and 425 nm (Fig. 4). A weaker fluorescence appeared when the sample was excited between 325 and 375 nm and the emission was monitored between 380 and 480 nm. In addition, the second emission band is located between 600 and 725 nm for the excitation between 300 and 325 nm. As the extension of this study in Fig. 5A, we present a comparison between the absorption and excitation spectra of **4** in acetonitrile. The excitation spectra of **4**

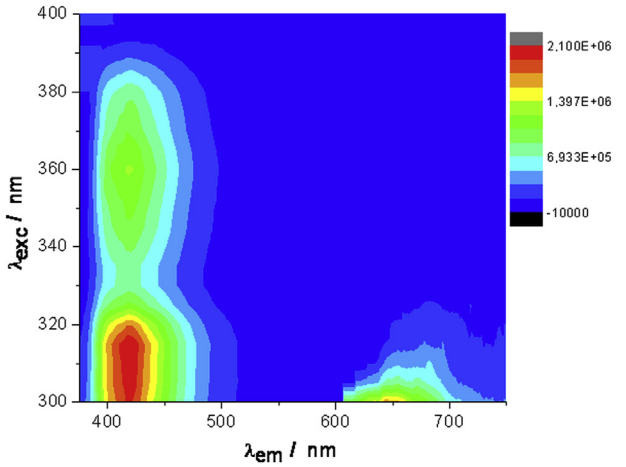

Fig. 4. Excitation-emission contour map of **4** in acetonitrile.

was recorded at 430 nm and 750 nm as emission wavelengths appeared at concentrations from the range 1.37×10^{-6} M and 1.83×10^{-5} M. The corresponding spectra of fluorescence excitation and absorption match each other. The only exception appears in the concentration of 1.83×10^{-5} M at about 600 nm, where some changes in the relative band intensities are observed. We believe that it might be due to the presence of weakly emitted dimers of **4**. The indications that dimers may be formed in solutions have been found for some azaphthalocyanines [30]. In Fig. S4C (see Supplementary Content) a plot of the absorbance vs. concentration at $\lambda = 500$ nm is presented. According to this data, two different linear correlations were found, the first in the range of concentrations from 1.37×10^{-6} M to 4.29×10^{-6} M with $R^2 = 0.996$ and the second from 4.86×10^{-6} M to 1.83×10^{-5} M with $R^2 = 0.999$. For lower concentrations only a monomeric form was present. However, we believe that at higher concentrations, the dimer (or even a higher aggregate) of **4** is present, apart from the monomer. In Fig. S4A and S4B (see Supplementary Content) the plots of absorbance vs. concentration of **4** at $\lambda = 380$ nm and 670 nm, respectively, were included. Summarizing, in the same range of concentrations of **4** two different linear correlations, namely at $\lambda = 380$ nm and 670 nm in the range of concentrations from 1.37×10^{-6} M to 4.29×10^{-6} M with $R^2 = 0.998$ and the second form 4.86×10^{-6} M to 1.83×10^{-5} M with $R^2 = 0.999$, were found. Further, the fluorescence excitation spectrum at $\lambda_{em} = 430$ nm was recorded. In Fig. 5B the excitation spectra of **4** at concentrations equal to 1.37×10^{-6} M and 1.83×10^{-5} M recorded at $\lambda_{em} = 430$ nm were presented. The fluorescence excitation spectra were compared to the absorption spectrum of **4** in the Soret-band region. Generally, we noted satisfactory agreement between the excitation spectrum and the Soret band in the absorption spectrum, which particularly match each other at ca. 380 nm.

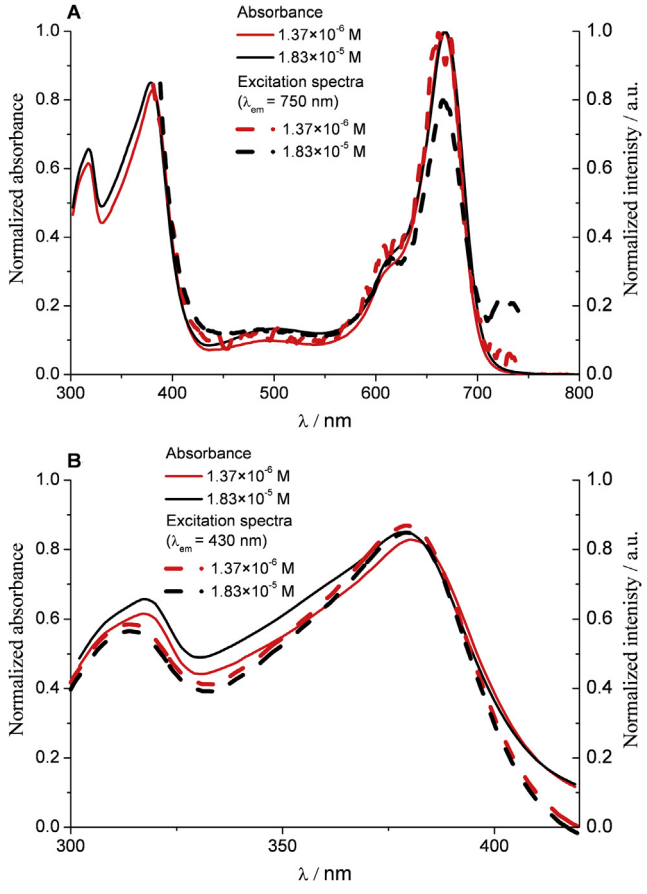

Fig. 5. Normalized absorption and excitation spectra A: $\lambda_{em} = 750$ nm and B: $\lambda_{em} = 430$ nm in acetonitrile for **4** at concentration 1.37×10^{-6} M and 1.83×10^{-5} M.

The fluorescence quantum yields (Φ_F) were calculated using the procedure described in the experimental part. The data for the S_2 emission are listed in Table 1 in selected organic solvents. Summarizing, the S_2 emission was found to be rather weak in all of the solvents used, with quantum yields of only about 10^{-4}, except for **4** in acetonitrile, where the quantum yield achieves 0.005. In addition, the fluorescence quantum yields for S_1 emission are presented. The values of Φ_F ($S_1 \rightarrow S_0$) are rather low, at about 10^{-3}, with the highest value determined in acetonitrile, and the lowest in acetone. The low values of fluorescence quantum yields might be explained by the presence of eight sulfur atoms in **4**, responsible for heavy-atom deactivation of the excited states. Notably, the relatively low fluorescence quantum yields were also found for zinc(II) phthalocyanine functionalized by eight thioglucose units [31]. Similarly, the influence of sulfur present in the phthalocyanine ring has been observed for octaglucosylated zinc(II) phthalocyanines, containing oxygen or sulfur bridges. In that case, fluorescence quantum yields were lower in derivatives containing sulfur bridges, than the oxygen bridged analogue [32].

In addition, the fluorescence lifetimes for S_1 emission in methanol and acetonitrile and for S_2 emission in acetonitrile were measured. In acetonitrile, the excitation at 380 nm was used and emission monitored at 427 nm. Mono-exponential fluorescence decay was observed with $\tau_{F\ (S2 \rightarrow S0)} = 3$ ps. As IRF (Instrument Response Function) was used xanthione in acetonitrile ($\tau_R = 12$ ps, $\lambda_{em} = 460$ nm) [33]. Such a short lifetime can be attributed to the S_2 state of **4**. Moreover, the fluorescence decay of **4** in acetonitrile at $\lambda_{exc} = 380$ nm and $\lambda_{em} = 690$ nm was accompanied by bi-exponential decay with $\tau_{F1\ (S1 \rightarrow S0)} = 32.4$ ps (40%) and $\tau_{F2\ (S1 \rightarrow S0)} = 105.6$ ps (60%). Similarly, in methanol bi-exponential decay with $\tau_{F1\ (S1 \rightarrow S0)} = 38.5$ ps (40%) and $\tau_{F2\ (S1 \rightarrow S0)} = 116.8$ ps (60%) was noted. Literature data indicates for some phthalocyanines and porphyrazines mono-exponential decay of the S_1 state on the ns time scale [31,32]. However, bi-exponential fluorescence decay was also noted for porphyrazines with peripheral 2,5-dimethylpyrrol-1-yl and dimethylamino groups dissolved in DMSO. The exact values of the fluorescence lifetimes were 1.24 ns (13%) and 2.95 ns (87%) for porphyrazine that was metalated with Mg ion. The origin of the shorter component can be a result of interaction between solvent (DMSO) and the metal cation at the centre of the macrocycle [16]. The data collected in Fig. S4 (see

Supplementary Content) and the decay contributions (in both cases 40%), indicate that the short-living species observed at λ_{em} = 690 nm are the dimers. The fluorescence lifetimes were measured at about 4 × 10^{-6} M (in acetonitrile) and at about 4.5 × 10^{-6} M (in methanol).

3.2. Solvatochromic studies

The Δ*f* solvent polarity scale was used to study the influence of the solvent polarity on the spectral and photophysical properties of **4**. The Δ*f* solvent polarity scale is based on the Onsager's reaction field theory and includes general solvent effects, including non-specific interactions between solutes and solvents of electrostatic and dispersive origin, arising from solvents acting as a dielectric continuum and specific solute − solvent interactions such as hydrogen bonding. The function describing the Δ*f* solvent polarity scale is based on Lippert-Mataga solvent polarity function [34,35]:

$$\Delta f = \frac{\varepsilon - 1}{2\varepsilon + 1} - \frac{n^2 - 1}{2n^2 + 1} \quad (3)$$

The Δ*f* parameter is accurately determined for most of the solvents and is dependent on the dielectric constant ε and the refractive index *n*.

A more detailed analysis was performed using seventeen different solvents, including cyclohexane, 1,4-dioxane, ethyl acetate, dichloroethane, dichloromethane, dimethyl sulfoxide, dimethylformamide, acetone, acetonitrile, 1-hexanol, 1-pentanol, 2-butanol, 1-butanol, 2-propanol, 1-propanol, ethanol and methanol. However, this analysis did not provide useful correlations (plots not shown). Using the regression of the ν_{abs} (Q-band) vs. Δ*f*, the correlation coefficient R = 0.33 was obtained for all solvents; separately, R = 0.56 was obtained for protic solvents (alcohols) and R = 0.65 for aprotic solvents. Using the regression of ν_{em} (in cm^{-1}) vs. the Δ*f*, R = 0.57 was obtained for all solvents, with slightly better correlations for the two separate groups of protic and aprotic solvents, R = 0.61 and 0.71, respectively.

Additionally for **4**, we used the four-parameter scale proposed by Catalán [36], see Table S3 in Supplementary Content. The four-parameter Catalán scale describes separately specific and non-specific interactions between solvents and solutes. The Catalán scale is based on specific and general scales, using four parameters (SA − solvent acidity, SB − solvent basicity, SdP − solvent dipolarity and SP − solvent polarizability scales) [36].

$$A = A_0 + a_{SP}SP + b_{SdP}SdP + c_{SA}SA + d_{SB}SB \quad (4)$$

Here, A_0 is the statistical quantity corresponding to the value of the property in the gas phase; *SP*, *SdP*, *SA*, and *SB*, represent solvent parameters, and a_{SP}, b_{SdP}, c_{SA}, and d_{SB} are the regression coefficients (solvent-independent), describing the sensitivity of the property *A* to the different solute–solvent interaction mechanisms [36]. In Table S3 (Supplementary Content) results of the regression calculations for the multilinear regression analysis of the absorption and emission maxima (in cm^{-1}) were presented. The parameter values of the gas phase (A_0) and the estimated coefficients: a_{SP}, b_{SdP}, c_{SA}, and d_{SB} with the correlation coefficient (R) were included. To summarize, the absorption maxima are mostly affected by basicity of solvents and solvent dipolarity with the R = 0.81. A less acceptable correlation coefficient (R = 0.66) was obtained when all of the Catalán parameters (solvent acidity, basicity, dipolarity and polariazability) were considered. For the emission maxima, a less satisfactory correlation as compared to the absorption (R = 0.73) for three Catalán parameters: solvent polarizability, acidity and basicity, was obtained. Noteworthy, for all Catalán parameters R = 0.64, was found.

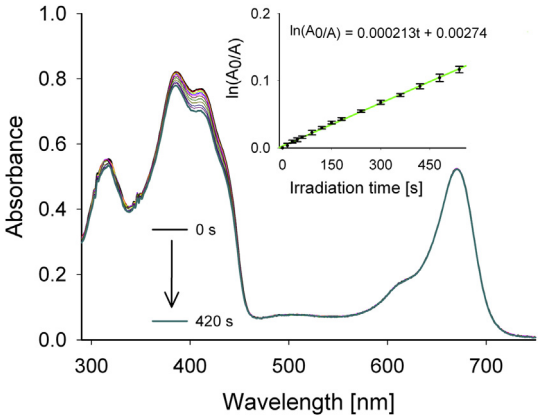

Fig. 6. Absorption spectra of a mixture of DPBF and **4** in DMF, during irradiation at 417 nm.

Solvatochromic studies for **4** in different solvents using various solvent polarity scales show that the correlations are rather poor. For such a large molecule as **4** with different groups, which are involved in specific and non-specific interactions, it is difficult to obtain satisfactory correlations (even when using various solvent polarity scales which include many types of interactions between solvents and solutes). Better correlations (R^2 = 0.925) were obtained in our previous study for 12 solvents when another phthalocyanine derivative bearing two 1-adamantylsulfanyl groups at peripheral positions was applied. At that time, we considered only the function of solvent refractive indices vs. Q-band maxima [37].

3.3. Singlet oxygen generation study and in vitro photodynamic activity results

The porphyrazine **4** generated singlet oxygen in DMF with a quantum yield of 0.02, with no significant photodegradation during the experiment (1.30 ± 0.01%). The absorption spectra indicating sensitized photooxidation of diphenylisobenzofurane (DPBF) are shown in Fig. 6.

To determine the cytotoxicity of the tested compound, the MTT assay for LNCaP prostate human cancer cell line was performed. The results show no cytotoxic potential of **4** in liposomal formulation. Moreover, a proliferative effect was observed after the PDT experiment, probably of hormetic nature.

Singlet oxygen luminescence photosensitized by **4** was observed in acetonitrile and dichloromethane, recording its characteristic spectra with a maximum at about 1270 nm. Measurements were done relative to the spectra of singlet oxygen obtained in acetonitrile and dichloromethane with perinaphtenone (Φ_Δ = 0.95 ± 0.05) [38] as a standard for excitation at 380 nm. Methylene blue was parallel utilized as a standard for excitation at 660 nm (Φ_Δ = 0.57 in dichloromethane and Φ_Δ = 0.52 in acetonitrile) [39,40]. In both solvents, acetonitrile and dichloromethane, the values of the quantum yield of singlet oxygen generated by **4** excited at 380 nm and 660 nm were 0.04 and 0.06, respectively.

4. Conclusions

A novel magnesium porphyrazine macrocycle was characterized in terms of its spectrochemical properties. Detailed emission studies were carried out, and its results permitted drawing a three dimensional map of excitation-emission properties. Porphyrazine exhibited interesting solvatochromic effects in the range of different solvents. Interestingly, the macrocycle generated singlet

oxygen upon excitation with visible light with low yield, thus when encapsulated in liposomes exhibited no photocytotoxity in the *in vitro* study on LNCaP cell line. The novel porphyrazine may be considered as a model compound for the series of its hyperbranched dendrimeric sulfur derivatives which will be reported on in due course and characterized in terms of their photochemical and biological activities.

Acknowledgments

This study was supported by the Polish National Science Centre under Grant No. 2012/05/E/NZ7/01204 and the European Fund for Regional Development No. UDA-POIG.02.01.00-30-182/09. Picosecond fluorescence decay measurements were made at the Center for Ultrafast Laser Spectroscopy at the Adam Mickiewicz University in Poznan, Poland.

Appendix A. Supplementary data

Supplementary data related to this article can be found at http://dx.doi.org/10.1016/j.dyepig.2014.10.004.

References

[1] Rodriguez-Morgade MS, Stuzhin PA. The chemistry of porphyrazines: an overview. J Porphyr Phthalocya 2004;8:1129–65.
[2] Cauchon N, Ali H, Hasséssian HM, van Lier JE. Structure–activity relationships of mono-substituted trisulfonated porphyrazines for the photodynamic therapy (PDT) of cancer. Photochem Photobiol Sci 2010;9:331–41.
[3] Zong H, Sun P, Mirkin CA, Barrett AGM, Hoffman BM. Varying the electrochemical potential and thickness of porphyrazine SAMs by molecular design. J Phys Chem B 2009;113:14892–903.
[4] Motyka M, Steer RP, Williams CC, Lee S, Ghiggino KP. Concerning the dual emission of porphyrazines employed in biomedical imaging. Photochem Photobiol Sci 2013;12:1086–90.
[5] Pietrangeli D, Rosa A, Ristori S, Salvati A, Altieri S, Ricciardi G. Carboranylporphyrazines and derivatives for boron neutron capture therapy: from synthesis to in vitro tests. Coord Chem Rev 2013;257:2213–31.
[6] Trivedi ER, Harney AS, Olive MB, Podgorski I, Moin K, Sloane BF, et al. Chiral porphyrazine near-IR optical imaging agent exhibiting preferential tumor accumulation. Proc Natl Acad Sci U S A 2010;107:1284–8.
[7] Vesper BJ, Lee S, Hammer ND, Elseth KM, Barrett AGM, Hoffman BM, et al. Developing a structure–function relationship for anionic porphyrazines exhibiting selective anti-tumor activity. J Photochem Photobiol B 2006;82:180–6.
[8] Lee S, Vesper BJ, Zong H, Hammer ND, Elseth KM, Barrett AGM, et al. Synthesis and biological analysis of thiotetra(ethylene glycol) monomethyl ether-functionalized porphyrazines: cellular uptake and toxicity studies. Metal-Based Drugs 2008;2008:391418. http://dx.doi.org/10.1155/2008/391418.
[9] Piskorz J, Skupin P, Lijewski S, Korpusinski M, Sciepura M, Konopka K, et al. Synthesis, physical–chemical properties and in vitro photodynamic activity against oral cancer cells of novel porphyrazines possessing fluoroalkylthio and dietherthio substituents. J Fluor Chem 2012;135:265–71.
[10] Michel SLJ, Hoffman BM, Baum SM, Barrett AGM. Peripherally functionalized porphyrazines: novel metallo macrocycles with broad, untapped potential. Prog Inorg Chem 2001;50:473–590.
[11] Ng ACH, Li XY, Ng DKP. Synthesis and photophysical properties of non-aggregated phthalocyanines bearing dendritic substituents. Macromolecules 1999;32:5292–8.
[12] Skupin-Mrugalska P, Piskorz J, Goslinski T, Mielcarek J, Konopka K, Düzgüneş N. Current status of liposomal porphyrinoid photosensitizers. Drug Discov Today 2013;18:776–84.
[13] Krystkowiak E, Dobek K, Maciejewski A. An intermolecular hydrogen-bonding effect on spectral and photophysical properties of 6-aminocoumarin in protic solvents. Photochem Photobiol Sci 2013;12:446–55.
[14] Ogunsipe A, Maree D, Nyokong T. Solvents effects on the photochemical and fluorescence properties of zinc phthalocyanine derivatives. J Mol Struct 2003;650:131–40.
[15] Karolczak J, Komar D, Kubicki J, Wrozowa T, Dobek K, Ciesielska B, et al. The measurements of picosecond fluorescence lifetimes with high accuracy and subpicosecond precision. Chem Phys Lett 2001;344:154–64.
[16] Sobotta L, Fita P, Szczolko W, Wrotynski M, Wierzchowski M, Goslinski T, et al. Functional singlet oxygen generators based on porphyrazines with peripheral 2,5-dimethylpyrrol-1-yl and dimethylamino groups. J Photochem Photobiol A 2013;269:9–16.
[17] Düzgüneş N. Preparation and quantitation of small unilamellar liposomes and large unilamellar reverse-phase evaporation liposomes. Methods Enzymol 2003;367:23–7.
[18] Wierzchowski M, Sobotta L, Skupin-Mrugalska P, Kruk J, Jusiak W, Yee M, et al. Phthalocyanines functionalized with 2-methyl-5-nitro-1H-imidazolylethoxy and 1,4,7-trioxanonyl moieties and the effect of metronidazole substitution on photocytotoxicity. J Inorg Biochem 2013;127:62–72.
[19] Abdelghany SM, Schmid D, Deacon J, Jaworski J, Fay F, McLaughlin KM, et al. Enhanced antitumor activity of the photosensitizer meso-tetra(N-methyl-4-pyridyl) porphine tetra tosylate through encapsulation in antibody-targeted chitosan/alginate nanoparticles. Biomacromolecules 2013;14:302–10.
[20] Zhu L, Lu M, Qu D, Wang Q, Tian H. Coordination-assembly for quantitative construction of bis-branched molecular shuttles. Org Biomol Chem 2011;9:4226–33.
[21] Gonca E, Gül A. Magnesium porphyrazinate with eight triphenylphosphonium moieties attached through (2-sulfanyl-ethoxycarbonyl-2-propyl) bridges. Inorg Chem Commun 2005;8:343–6.
[22] Ahsen V, Yılmazer E, Gürek A, Gül A, Bekaroğlu Ö. Synthesis and characterization of crown-ether-containing phthalocyanines with group-IV-A elements. Helv Chim Acta 1988;71:1616–21.
[23] Okur Aİ, Gül A, Cihan A, Tan N, Bekaroğlu Ö. Synthesis and properties of phthalocyanines substituted with four crown ethers. Synth React Inorg Met-Org Chem 1990;20:1399–412.
[24] Patra D, Barakat C. Synchronous fluorescence spectroscopic study of solvatochromic curcumin dye. Spectrochim Acta Mol Biomol Spectros 2011;79:1034–41.
[25] Patra D, Mishra AK. Recent developments in multi-component synchronous fluorescence scan analysis. TrAC-Trend Anal Chem 2002;21:787–98.
[26] Prukala D, Prukala W, Gierszewski M, Karolczak J, Khmelinskii I, Sikorski M. Influence of pH on photophysical properties of (E)-1-(4-chlorobenzyl)-4-(4-hydroxystyryl)pyridinium chloride. Photochem Photobiol Sci 2012;11:1454–64.
[27] Prukala D, Sikorska E, Koput J, Khmelinskii I, Karolczak J, Gierszewski M, et al. Acid–base equilibriums of lumichrome and its 1-methyl, 3-methyl, and 1,3-dimethyl derivatives. J Phys Chem A 2012;116:7474–90.
[28] Gan Q, Xiong F, Li SY, Wang SQ, Shen SY, Xu HJ, et al. Synthesis and photophysical properties of a series of octaphenyl-porphyrazine–magnesium. Inorg Chem Commun 2005;8:285–8.
[29] Ehrlich LA, Skrdla PJ, Jarrell WK, Sibert JW, Armstrong NR, Saavedra SS, et al. Preparation of polyetherol-appended sulfur porphyrazines and investigations of peripheral metal ion binding in polar solvents. Inorg Chem 2000;39:3963–9.
[30] Musil Z, Zimcik P, Miletin M, Kopecky K, Petrik P, Lenco J. Influence of electron-withdrawing and electron-donating substituents on photophysical properties of azaphthalocyanines. J Photochem Photobiol A 2007;186:316–22.
[31] Aggarwal A, Singh S, Zhang Y, Anthes M, Samaroo D, Gao R, et al. Synthesis and photophysics of an octathioglycosylated zinc(II) phthalocyanine. Tetrahedron Lett 2011;52:5456–9.
[32] Iqbal Z, Ogunsipe A, Nyokong T, Lyubimtsev A, Hanack M, Ziegler T. Photophysics and photochemistry of octaglucosylated zinc phthalocyanine derivatives. J Porphyr Phthalocya 2012;16:413–22.
[33] Lorenc M, Maciejewski A, Ziolek M, Naskrecki R, Karolczak J, Kubicki J, et al. Mechanism and deactivation kinetics of S_2-xanthione in acetonitrile, a quenching solvent, and of S_2-exciplex measured by pico- and femtosecond laser spectroscopy. Chem Phys Lett 2001;346:224–32.
[34] Lakowicz JR. Principles of fluorescence spectroscopy. 2nd ed. New York: Kluwer Academic/Plenum Publishers; 1999.
[35] Lippert E. Spektroskopische bestimmung des dipolmomentes aromatischer verbindungen im ersten angeregten singulettzustand. Zeit Elektrochem 1957;61:962–75.
[36] Catalán J. Toward a generalized treatment of the solvent effect based on four empirical scales: dipolarity (SdP, a new scale), polarizability (SP), acidity (SA), and basicity (SB) of the medium. J Phys Chem B 2009;113:5951–60.
[37] Kryjewski M, Nowak M, Kasprzycki P, Fita P, Radzewicz C, Goslinski T, et al. Synthesis and photochemical properties of unsymmetrical phthalocyanine bearing two 1-adamantylsulfanyl groups at adjacent peripheral positions. Inorg Chem Commun 2013;27:56–9.
[38] Schmidt R, Tanielian C, Dunsbach R, Wolff C. Phenalenone, a universal reference compound for the determination of quantum yields of singlet oxygen (Delta) sensitization. J Photochem Photobiol A 1994;79:11–7.
[39] Chin K, Trevithick-Sutton C, McCallum J, Jockusch S, Turro NJ, Scaiano JC, et al. Quantitative determination of singlet oxygen generated by excited state aromatic amino acids, proteins, and immunoglobulins. J Am Chem Soc 2008;130:6912–3.
[40] Cakmak Y, Kolemen S, Duman S, Dede Y, Dolen Y, Kilic B, et al. Designing excited states: theory-guided access to efficient photosensitizers for photodynamic action. Angew Chem Int Ed 2011;50:11937–41.